(3) Lee, C. W.; Chen, X.; Kevan, L. *J. Phys. Chem.* **1992,** *96,* 357.
(4) Zamadics, M.; Chen, X.; Kevan, L. *J. Phys. Chem.* **1992,** *96,* 2652.
(5) Wilson, S. T.; Lok, B. M.; Messina, C. A.; Cannon, T. R.; Flanigen, E. M. *J. Am. Chem. Soc.* **1982,** *104,* 1146.
(6) Packet, D.; Dehertogh, W.; Schoonheydt, R. A. In *Zeolites: Synthesis, Structure, Technology and Applications*; Drzaj, B., Hoeevar, S., Pejovnik, S., Eds.; Elsevier: Amsterdam, 1985; pp 351-358.
(7) Pluth, J. J.; Smith, J. V.; Mortier, W. J. *Mater. Res. Bull.* **1977,** *12,* 1001.
(8) Choa, C.; Lunsford, J. H. *J. Chem. Phys.* **1973,** *59,* 3920.
(9) Sass, C.; Kevan, L. *J. Phys. Chem.* **1989,** *93,* 4669.
(10) Anderson, M. W.; Kevan, L. *J. Phys. Chem.* **1986,** *90,* 6452.
(11) Anderson, M. W.; Kevan, L. *J. Phys. Chem.* **1987,** *91,* 2926.
(12) Dryer, A. An *Introduction to Zeolite Molecular Sieves*; Wiley: New York, 1988; p 17.
(13) Smith, J. V. *Acta Crystallogr.* **1962,** *15,* 835.
(14) Kevan, L. In *Modern Pulsed and Continuous-Wave Electron Spin Resonance*; Kevan, L., Bowman, M. K., Eds.; Wiley: New York, 1990; pp 231-266.
(15) Kevan, L. In *Time Domain Electron Spin Resonance*; Kevan, L., Schwartz, R. N., Eds.; Wiley: New York, 1979; pp 279-341.
(16) Dikanov, S. A.; Shubin, A. A.; Parmon, V. N. *J. Magn. Reson.* **1981,** *42,* 474.
(17) Calligaris, M.; Nardin, G. *Zeolites* **1982,** *2,* 200.

(18) Hathaway, B. J.; Billing, D. E. *Coord. Chem. Rev.* **1970,** *5,* 143.
(19) Narayana, M.; Kevan, L. In *Proceedings of the Sixth International Zeolite Conference*; Bissio, A., Olson, D. H., Eds.; Butterworth: London, 1984; p 774.
(20) Narayana, M.; Kevan, L. *J. Chem. Soc., Faraday Trans 1* **1986,** *82,* 213.
(21) Anderson, M.; Kevan, L. *J. Phys. Chem.* **1987,** *91,* 4147.
(22) Flanigen, E. M.; Lok, B. M.; Patton, R. L.; Wilson, S. T. *Pure Appl. Chem.* **1986,** *58,* 1351.
(23) Breck, D. W. *Zeolite Molecular Sieves: Structure, Chemistry, and Use*; Wiley: New York, 1974; pp 107-110.
(24) Anderson, M.; Kevan, L. *J. Phys. Chem.* **1986,** *90,* 3206.
(25) Anderson, M.; Kevan, L. In *Perspectives in Molecular Sieve Science*; Flank, W. H., Whyte, T. E. Jr., Eds.; ACS Symposium Series 368; American Chemical Society: Washington, DC, 1988; p 150.
(26) Sass, C.; Kevan, L. *J. Phys. Chem.* **1988,** *92,* 5219.
(27) Lee, H.; Narayana, M.; Kevan, L. *J. Phys. Chem.* **1985,** *89,* 2419.
(28) Alberti, A.; Galli, E.; Vezzalini, G.; Passaglia, E.; Zanazzi, P. F. *Zeolites* **1982,** *2,* 303.
(29) Szostak, R. *Molecular Sieves: Principles of Synthesis and Identification*; Van Nostrand Reinhold: New York, 1989; pp 30-35.
(30) Datka, J *J. Chem. Soc., Faraday Trans. 1* **1981,** *77,* 511.
(31) Kevan, L. *Rev. Chem. Intermed.* **1987,** *8,* 53.
(32) Ichikawa, T.; Kevan, L. *J. Am. Chem. Soc.* **1981,** *103,* 5355.

Charge and Spin Density Waves in the Electronic Structure of Graphite. Application to Analysis of STM Images

Andrei L. Tchougreeff[†] and Roald Hoffmann*

Department of Chemistry and Materials Science Center, Cornell University, Baker Laboratory, Ithaca, New York 14853-1301 (Received: May 4, 1992; In Final Form: June 22, 1992)

On the basis of the electronic structure of a graphite monolayer, represented in the unrestricted Hartree–Fock approximation by an extended Hubbard Hamiltonian, we interpret the data on observed scanning tunneling microscopy (STM) images of bulk graphite, graphite monolayers on Pt(111) and graphite intercalation compounds. The well-known (and puzzling) pattern of graphite STM images, with only three of the six atoms of each carbon hexagon visible, is tentatively explained by the intrinsic features of the electronic structure of a graphite monolayer, without invoking well-known explanations attributing the observed effect to structural differences between the sites and to interlayer interactions. In particular we construct a phase diagram for graphite in the space defined by the magnitude of on-site and nearest-neighbor electron repulsions. The conditions for insulating charge and spin density wave solutions are delineated. A charge density wave state, which we estimate is reasonable for the graphite monolayer, would give the 3-fold STM image. A spin density wave state, which we think somewhat less likely, will also give unequal tunneling currents from A and B sites of graphite monolayer, provided the STM tip carries a local magnetic moment.

Introduction

Graphite, the simplest quasi-two-dimensional crystal, has been studied for many years, both theoretically and experimentally.[1,2] One recent source of interest in graphite is its formation during hydrocarbon decomposition on different metal surfaces.[3,4]

The surface of graphite has been the subject of many scanning tunneling microscopy (STM) investigations.[5-8] In most STM images of graphite one observes only three of the six carbon atoms forming the well-known carbon hexagons of the graphite lattice. This feature is usually explained by interactions of the surface layer with underlying two-dimensional graphite layers. The structure of graphite (Figure 1) is such that the interactions between the layers make the carbon atoms of the surface layer nonequivalent. The A-type carbon atoms have an atom from another layer immediately under them, whereas the B-type atoms are located above the centers of the hexagons of the layer beneath. Atoms of only one of these two types are believed to be observed in the STM images of surfaces of graphite.[5] We might note here, that in the atomic force microscope (AFM), depending on the experimental conditions, sometimes all six and sometimes only three of the ring carbons are imaged.[9]

However, almost at the same time as this explanation was forming, Tersoff[10] proposed an alternative origin for the observed STM image of graphite. The single graphite layer has a zero energy gap between the occupied and empty band. For that reason some perturbed states with lower symmetry and different charges on the A and B carbon atoms may have lower energy than the ideal graphite monolayer. The charge asymmetry in its turn can produce the observed graphite STM images.

This idea is ingenious but nevertheless encounters some problems. Already in the pioneering work by Slonczewski and Weiss[11] and by McClure[12] on the electronic structure of graphite, it was shown that in bulk (three-dimensional) graphite the interlayer electron transfer integrals give a finite Fermi surface. So the simple arguments of Tersoff[10] do not apply in the strict sense. No specific interaction which would be responsible for the charge wave formation was proposed by Tersoff.[10] Moreover, some recent LDA calculations[13,14] on the electronic structure of the surface of bulk graphite show that the charge on the A and B sites in the surface layer is in fact different because of interaction with the layer beneath. It has also been predicted[13,14] that this asymmetry should disappear in graphite intercalation compounds, where the structural difference between carbon atoms disappears as well.

---

†On leave from the L.Y. Karpov Institute of Physical Chemistry, Moscow, Russia.
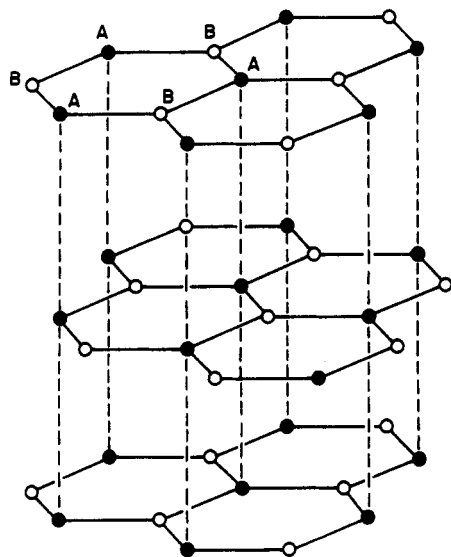
Figure 1. Fragment of the three-dimensional graphite crystal. The A-type atoms (solid circles) have a carbon atom in the layer directly below, while the B-type carbon atoms (open circles) do not have any atom in the layer below.

Despite these uncertainties Tersoff's idea is very attractive. Moreover, some recent data support it. It has been observed that a graphite monolayer forms on the Pt(111) surface.[15] In the high-resolution STM images of that monolayer only three of the six carbon atoms of any hexagon are observed, though there are no structural reasons for any difference between the A and B sites in such a graphite on Pt(111) overlayer.

This recent observation makes us think that the explanation of nonequivalency of the A and B sites given by Tersoff[10] in terms of the intrinsic electronic structure of a graphite monolayer is generally correct. However, a closer discussion is needed to cope with the problems outlined above.

This we will provide. In the present paper we treat the graphite monolayer in the tight binding approximation (see ref 16; a recent review of applications of the tight-binding approximation to chemical problems is given in ref 17). We restrict ourselves to the π-electrons of a graphite monolayer.[11,12,18] To reproduce the charge density state of the graphite monolayer we describe its π-electrons by the extended Hubbard model, which is known to be sufficient for description of different unsymmetrical states in extended conjugated systems (polyene, carbyne[19]).

Extended Hubbard Model for Graphite Monolayer

The simplest theoretical model developed for conjugated systems is the well-known Hückel method.[20] In the framework of that method one looks only at the π orbitals ($2p_z$ orbitals of carbon atoms; the z axis chosen normal to the plane formed by the carbon atoms of the system). The model Hamiltonian of the Hückel method includes only one-electron terms describing electron transfers between $2p_z$ orbitals on adjacent sites.

The Hückel model is enormously successful. It suffices to say that it describes almost all aspects of structure and reactivity of aromatic compounds (see, for example, ref 21). However, there are limitations to the Hückel model. In our case we are interested in the charge distribution in a graphite monolayer. To describe such a layer properly electron–electron interactions must be included. The simplest model taking into account electron–electron interactions neglected in the Hückel model is the Hubbard model.[22] It is obtained from the Hückel model by adding the Coulomb interaction in an extremely reduced form: only between π-electrons occupying the same site and having opposite spin projections (for review see refs 22 and 23). The possible ground states of conjugated systems are quite limited in the Hubbard model. They include a uniform (or metallic) ground state (where all the elements of the density matrix do not depend on the site) and a ground state with a spin density wave (SDW), where the average spin projection has opposite signs on adjacent sites.
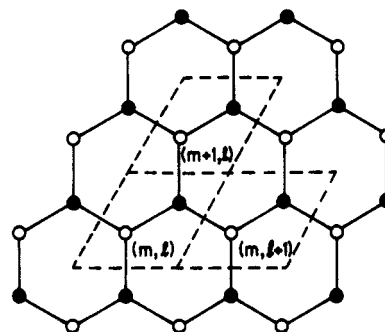
Figure 2. Structure of a graphite monolayer.

The model Hamiltonian becomes more flexible and allows a ground state with a nonuniform charge distribution (the charge density wave state, CDW) when repulsion between electrons occupying adjacent sites is added.[19] The long-range tail of the Coulomb interaction between electrons adds nothing new to the model with repulsion between electron occupying the same and adjacent sites only[24] (the extended Hubbard model). We will use this model in the present paper in order to describe possible ground states of the graphite monolayer.

The structure of the two-dimensional graphite monolayer is shown in Figure 2. The unit cell contains two equivalent carbon atoms A and B. The integer numbers (m,l) denote the coordinates of the unit cell. Let $a_{ml\sigma}$ and $b_{ml\sigma}$ be the operators annihilating electrons with spin projection $\sigma = \pm^1/_2$ on the A and B sites, respectively, in the (m,l)-th unit cell. Using these operators we can write the extended Hubbard Hamiltonian for the graphite monolayer:

$$H = -\beta\sum_{\substack{m,l \\ \sigma}}(a^+_{ml\sigma}b_{ml\sigma} + b^+_{ml\sigma}a_{m+1l\sigma} + b^+_{ml\sigma}a_{ml+1\sigma} + \text{h.c.}) +$$

$$\gamma_0\sum_{m,l}(a^+_{ml\uparrow}a_{ml\uparrow}a^+_{ml\downarrow}a_{ml\downarrow} + b^+_{ml\uparrow}b_{ml\uparrow}b^+_{ml\downarrow}b_{ml\downarrow}) +$$

$$\gamma_1\sum_{\substack{m,l \\ \sigma,\sigma'}} (a^+_{ml\sigma}a_{ml\sigma}b^+_{ml\sigma'}b_{ml\sigma'} + b^+_{ml\sigma}b_{ml\sigma}a^+_{m+1l\sigma'}a_{m+1l\sigma'} +$$

$$b^+_{ml\sigma}b_{ml\sigma}a^+_{ml+1\sigma'}a_{ml+1\sigma'}) - 3\gamma_1\sum_{\substack{m,l \\ \sigma}}(a^+_{ml\sigma}a_{ml\sigma} + b^+_{ml\sigma}b_{ml\sigma}) \quad (1)$$

The first term (proportional to β) is the Hückel Hamiltonian for the graphite monolayer. It describes electron transfer from A and B sites in the (m,l)-th unit cell to adjacent sites both inside and outside the unit cell. The second term (proportional to γ_0) is the Hubbard term. It describes repulsion between electrons when they happen to occupy the same site. The third term (proportional to γ_1) describes the repulsion between electrons occupying adjacent sites. The last term describes the attraction of electrons to the cores of the adjacent carbon atoms. The attraction energy is set equal to the intersite electron repulsion parameter, as in the PPP method.[25]

To find the ground state of a graphite monolayer described by the Hamiltonian eq 1, we use the equation of motion method (in the context of conjugated systems see the description of this method in refs 18, 19, 22, and 24). It is based on the Heisenberg representation, which ascribes the time dependence to operators

$$i\ \partial a_{ml\sigma}/\partial t = [a_{ml\sigma},H] \qquad i\ \partial b_{ml\sigma}/\partial t = [b_{ml\sigma},H]$$

Inserting the Hamiltonian eq 1 into these general formulas and making use of the fermion anticommutation relations, we get

$$i\ \partial a_{ml\sigma}/\partial t = -\beta(b_{ml\sigma} + b_{m-1l\sigma} + b_{ml-1\sigma}) + \gamma_0 a^+_{ml-\sigma}a_{ml-\sigma}a_{ml\sigma} +$$

$$\gamma_1\sum_{\sigma'}(b^+_{ml\sigma'}b_{ml\sigma'} + b^+_{m-1l\sigma'}b_{m-1l\sigma'} + b^+_{ml-1\sigma'}b_{ml-1\sigma'})a_{ml\sigma} - 3\gamma_1 a_{ml\sigma}$$

$$i\ \partial b_{ml\sigma}/\partial t = -\beta(a_{ml\sigma} + a_{m+1l\sigma} + a_{ml+1\sigma}) + \gamma_0 b^+_{ml-\sigma}b_{ml-\sigma}b_{ml\sigma} +$$

$$\gamma_1\sum_{\sigma'}(a^+_{ml\sigma'}a_{ml\sigma'} + a^+_{m+1l\sigma'}a_{m+1l\sigma'} + a^+_{ml+1\sigma'}a_{ml+1\sigma'})b_{ml\sigma} - 3\gamma_1 b_{ml\sigma}$$

$$(2)$$

The solutions of the equations of motion are defined by the condition

$$i\,\partial F/\partial t = [F,H] = \epsilon F$$

So we must find a set of one-electron operators F such that their commutator with the Hamiltonian is proportional to themselves. Unfortunately this problem cannot be solved in the above form because of the three-fermion products present in the right-hand parts of the equations of motion. At this stage we apply the Hartree–Fock approximation, which consists in substitution of an expression containing averages over the ground state instead of the three-fermion products:

$$c_1^+ c_2 c_3 \rightarrow \langle c_1^+ c_2 \rangle c_3 - \langle c_1^+ c_3 \rangle c_2$$

The general form of the averages $\langle ... \rangle$ is usually chosen on the basis of physical assumptions. In our particular case we assume the averages to have the symmetry of the original lattice, so both the total charge and total magnetic moment of any unit cell are zero. That assumption leads us to the following form of the "on-site" averages:

$$\langle a_{ml\sigma}^+ a_{ml\sigma}\rangle = \tfrac{1}{2} + \delta_\sigma \qquad \langle b_{ml\sigma}^+ b_{ml\sigma}\rangle = \tfrac{1}{2} - \delta_\sigma \qquad (3)$$

where the parameters δ_σ must be determined from self-consistency conditions (see below). The averages of the electron transfer operators of the form $\langle a_\sigma^+ b_\sigma\rangle$ are set to P_σ for all adjacent sites, both intracell and intercell ones. To ensure the conservation of the projection of the total spin of the system, the averages of the form $\langle c_\sigma c_{-\sigma}\rangle$ are set to zero.

After the Hartree–Fock approximation is applied and the averages in the above form are inserted, the equations of motion for the one-electron operators become

$$i\,\partial a_{ml\sigma}/\partial t = -(\beta + \gamma_1 P_\sigma)(b_{ml\sigma} + b_{m-1l\sigma} + b_{ml-1\sigma}) +$$
$$(\gamma_0/2 + \gamma_0\delta_{-\sigma} - 3\gamma_1(\delta_\uparrow + \delta_\downarrow))a_{ml\sigma}$$

$$i\,\partial b_{ml\sigma}/\partial t = -(\beta + \gamma_1 P_\sigma)(a_{ml\sigma} + a_{m+1l\sigma} + a_{ml+1\sigma}) +$$
$$(\gamma_0/2 - \gamma_0\delta_{-\sigma} + 3\gamma_1(\delta_\uparrow + \delta_\downarrow))b_{ml\sigma} \quad (4)$$

Now the equations become linear, at least formally (δ_σ and P_σ themselves depend on the solution of these equations), and can be solved by Fourier transformation. The Fourier transforms of the site operators are

$$a_{k\sigma} = (1/N)\sum_{m,l}\exp(-ik_x m - ik_y l)a_{ml\sigma}$$

$$b_{k\sigma} = (1/N)\sum_{m,l}\exp(-ik_x m - ik_y l)b_{ml\sigma}$$

$\mathbf{k} = (k_x, k_y)$ is the wave vector, N is the number of unit cells in both directions. The equations of motion become

$$i\,\partial a_{k\sigma}/\partial t = -(\beta + \gamma_1 P_\sigma)(1 + e^{ik_x} + e^{ik_y})b_{k\sigma} +$$
$$(\gamma_0/2 + \gamma_0\delta_{-\sigma} - 3\gamma_1(\delta_\uparrow + \delta_\downarrow))a_{k\sigma}$$

$$i\,\partial b_{k\sigma}/\partial t = -(\beta + \gamma_1 P_\sigma)(1 + e^{-ik_x} + e^{-ik_y})a_{k\sigma} +$$
$$(\gamma_0/2 - \gamma_0\delta_{-\sigma} + 3\gamma_1(\delta_\uparrow + \delta_\downarrow))b_{k\sigma} \quad (5)$$

So we have a system of $4N^2$ linear equations which are connected pairwise only—for the same values of $\mathbf{k}$ and σ. The solution of these equations can be written in the form

$$f_{k\sigma} = x_{k\sigma}a_{k\sigma} + y_{k\sigma}b_{k\sigma}$$

$$g_{k\sigma} = -y_{k\sigma}^* a_{k\sigma} + x_{k\sigma}b_{k\sigma}$$

$$|x_{k\sigma}|^2 + |y_{k\sigma}|^2 = 1$$

Corresponding orbital energies are

$$\epsilon_{k\sigma}^\pm = \gamma_0/2 \pm R_{k\sigma}$$

$$R_{k\sigma} = ((\gamma_0\delta_{-\sigma} - 3\gamma_1(\delta_\uparrow + \delta_\downarrow))^2 + (\beta + \gamma_1 P_\sigma)^2\epsilon_0^2(\mathbf{k}))^{1/2}$$

$$\epsilon_0^2(\mathbf{k}) = 3 + 2\cos k_x + 2\cos k_y + 2\cos(k_x - k_y) \quad (6)$$

All the states corresponding to the minus sign (f states) are occupied. The averages can be expressed as integrals over the occupied orbitals:

$$\langle a_{ml\sigma}^+ a_{ml\sigma}\rangle = \tfrac{1}{2} + \delta_\sigma = (1/4\pi^2)\int_{-\pi}^{\pi}\int_{-\pi}^{\pi}|x_{k\sigma}|^2\,dk_x\,dk_y$$

$$\langle b_{ml\sigma}^+ b_{ml\sigma}\rangle = \tfrac{1}{2} - \delta_\sigma = (1/4\pi^2)\int_{-\pi}^{\pi}\int_{-\pi}^{\pi}|y_{k\sigma}|^2\,dk_x\,dk_y$$

$$\langle a_{ml\sigma}^+ b_{mm\sigma}\rangle = \langle b_{ml\sigma}^+ a_{ml+1\sigma}\rangle = \langle b_{ml\sigma}^+ a_{m+1l\sigma}\rangle = P_\sigma$$

$$P_\sigma = (1/4\pi^2)\int_{-\pi}^{\pi}\int_{-\pi}^{\pi}x_{k\sigma}y_{k\sigma}^*\,dk_x\,dk_y \quad (7)$$

The coefficients $x_{k\sigma}$ and $y_{k\sigma}$ satisfy the conditions

$$|x_{k\sigma}|^2 - |y_{k\sigma}|^2 = -\frac{\gamma_0\delta_{-\sigma} - 3\gamma_1(\delta_\uparrow + \delta_\downarrow)}{R_{k\sigma}}$$

$$x_{k\sigma}y_{k\sigma}^* = \frac{(\beta + \gamma_1 P_\sigma)(1 + e^{-ik_x} + e^{-ik_y})}{R_{k\sigma}} \quad (8)$$

From these expressions we can get the self-consistency equations in closed form:

$$\delta_\sigma = -\frac{\gamma_0\delta_{-\sigma} - 3\gamma_1(\delta_\uparrow + \delta_\downarrow)}{8\pi^2}\int_{-\pi}^{\pi}\int_{-\pi}^{\pi}\frac{dk_x\,dk_y}{R_{k\sigma}}$$

$$P_\sigma = \frac{1}{8\pi^2}\int_{-\pi}^{\pi}\int_{-\pi}^{\pi}\frac{(\beta + \gamma_1 P_\sigma)(1 + e^{-ik_x} + e^{-ik_y})}{R_{k\sigma}}\,dk_x\,dk_y \quad (9)$$

Solutions of the latter system can be of two types. One of them corresponds to spin asymmetry of the A and B sites (SDW); another one corresponds to charge asymmetry between the sites (CDW). For the SDW case we have $\delta_\uparrow = -\delta_\downarrow = \delta$, and the self-consistency equation looks like

$$\delta = \frac{\gamma_0\delta}{8\pi^2}\int_{-\pi}^{\pi}\int_{-\pi}^{\pi}\frac{dk_x\,dk_y}{R_{k\sigma}} \quad (10)$$

This equation always has the trivial solution $\delta = 0$, corresponding to a uniform distribution of spin density. In that case, the orbital energies and expansion coefficients for the orbitals coincide with those obtained from the simple Hückel model[26] but with the electron transfer parameter β replaced by $(\beta + \gamma_1 P_\sigma)$. This solution corresponds to the metallic phase of the graphite layer. In the metallic phase the bond order does not depend on parameters of the Hamiltonian and is predetermined by the symmetry of the model[26] ($P_\sigma^M \approx 0.263$).

If $\delta \neq 0$ the self-consistency equation for δ takes the form

$$1 = \frac{\gamma_0}{8\pi^2}\int_{-\pi}^{\pi}\int_{-\pi}^{\pi}\frac{dk_x\,dk_y}{R_{k\sigma}} \quad (11)$$

One can hope to find its solutions with $\delta > 0$ only if the right-hand side is able to exceed unity.[18] The condition reads

$$1 \leq \frac{\gamma_0}{(\beta + \gamma_1 P_\sigma)}\frac{1}{8\pi^2}\int_{-\pi}^{\pi}\int_{-\pi}^{\pi}\frac{dk_x\,dk_y}{\epsilon_0(\mathbf{k})} \quad (12)$$

Though this condition depends on the bond order, which in principle must be determined self-consistently, it is also clear from eq 9 that the bond order parameter P_σ reaches its maximal value P_σ^M in the metallic phase. The latter value must be inserted in the definition of the critical interaction strength, because in the insulating phase the bond order is smaller and the condition eq 12 is satisfied there. This inequality is analogous to the condition for the existence of SDW in the Hubbard model,[18] to which it can be reduced by setting $\gamma_1 = 0$. For that case the above condition has been written[18]

$$\left(\frac{\gamma_0}{\beta}\right) \geq U_c = \left(\frac{1}{8\pi^2}\int_{-\pi}^{\pi}\int_{-\pi}^{\pi}\frac{dk_x\,dk_y}{\epsilon_0(\mathbf{k})}\right)^{-1} \approx 2.26$$
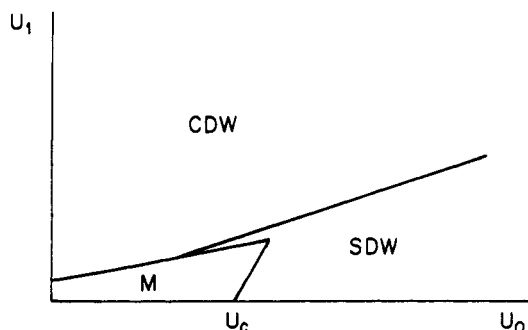
Figure 3. (U_0, U_1) phase diagram of graphite monolayer. The area where metallic graphite exists is bounded by the straight lines $U_0 = U_c(1 + P_\sigma^M U_1)$ and $6U_1 - U_0 = U_c(1 + P_\sigma^M U_1)$. The SDW and CDW regions are separated by the line $U_0/3 = U_1$ outside the metallic region.

In the extended Hubbard model this condition for the existence of the SDW solution can be simply rewritten as follows:

$$\left(\frac{\gamma_0}{\beta + \gamma_1 P_\sigma^M} \right) \geq U_c \qquad (13)$$

The bond order P_σ^M is positive, so the denominator in the above condition is always larger than that in the Hubbard model. Thus the electron–electron repulsion should be stronger for an SDW-type ground state to exist.

For the CDW case $\delta_\uparrow = \delta_\downarrow = \delta$. The general self-consistency equation (eq 9) for δ takes the form

$$\delta = -\frac{(\gamma_0 - 6\gamma_1)\delta}{8\pi^2} \int_{-\pi}^{\pi} \int_{-\pi}^{\pi} \frac{dk_x\, dk_y}{R_{k\sigma}} \qquad (14)$$

As in the case of the SDW self-consistency equation, the trivial solution $\delta = 0$ always exists. Nontrivial solutions with $\delta \neq 0$ are possible only if $6\gamma_1 - \gamma_0 > 0$. Like the SDW solutions, they are also conditioned by the relative strength of interaction compared to electron transfer. This condition reads

$$\left(\frac{6\gamma_1 - \gamma_0}{\beta + \gamma_1 P_\sigma} \right) \geq U_c \qquad (15)$$

Finally we obtain expressions for the electronic energy of graphite per atom in all three possible states:

$$E_M = -3\beta \sum_\sigma P_\sigma + \gamma_0/4 - 3\gamma_1 \sum_\sigma P_\sigma^2$$

$$E_{SDW} = -3\beta \sum_\sigma P_\sigma + \gamma_0/4 - \gamma_0 \delta^2 - 3\gamma_1 \sum_\sigma P_\sigma^2$$

$$E_{CDW} = -3\beta \sum_\sigma P_\sigma + \gamma_0/4 - (6\gamma_1 - \gamma_0)\delta^2 - 3\gamma_1 \sum_\sigma P_\sigma^2 \qquad (16)$$

Here the quantities describing the electron density (δ and P_σ) are to be found self-consistently.

We are now in a position to describe the phase diagram for the graphite monolayer in the coordinates $U_0 = \gamma_0/\beta$, $U_1 = \gamma_1/\beta$ (Figure 3). This drawing shows in what areas of the (U_0, U_1) plane SDW, CDW, or metallic (M) ground states are of lower energy. Both insulating states (SDW and CDW) always have lower energy than the metallic one, if they exist. Therefore the area where the metallic state exists is bounded by straight lines along which the inequalities of eqs 13 and 15 turn into equalities.

In the insulating region, where the electron–electron interactions are strong, the boundary between the SDW and CDW areas is determined by the condition $U_0 = 3U_1$. Along that line the contributions from electron–electron interactions to the total energy are equal for both SDW and CDW states. Above that line the CDW state has lower energy; below it the SDW state does.

We see that the type of ground state of the graphite monolayer—metallic or insulating—and the particular type of insulating state—with spin or with charge order—depends on the parameters of the model. Let us discuss now what the parameters of electron transfer and those of electron–electron interaction might be for graphite.

The electron-transfer parameter β is simplest to estimate. It is known to be 2.4–2.5 eV for small conjugated hydrocarbons such as benzene, naphthalene, etc., for carotenoids and for the infinite polyene used to mimic the organic conductor polyacetylene. We also assume this value, in line with refs 18, 19, 22, 25, and 26.

The electron–electron repulsion parameters present greater problems. Small conjugated molecules such as benzene can be perfectly described by the Pariser–Parr–Pople (PPP) method.[25] In the PPP method $\gamma_0 = 11.16$ eV and the Coulomb repulsion between electrons on different sites decreases as $1/R$, where R is the intersite separation. It is known, however, that the PPP method fails when the size of the conjugated system exceeds a certain critical value.[27] That happens because of electron correlation. These effects can be partially taken into account by adjustment of the interaction parameters. For instance, for a long time the infinite polyene had been well described[22] by the Hubbard model with γ_0 equal to only 6 eV. This adjustment has received some justification recently within the framework of the regular renormalization procedure[19] for the interaction parameters in large polyconjugated systems. It has been shown[28] that for long polyene molecules the original PPP-like long-range repulsion between electrons with an on-site value of about 11 eV is renormalized as follows: the on-site repulsion becomes about 7 eV, and the intersite repulsion now decreases steeply reaching a limiting value of about 2 eV over two or three interatomic separations. The constant limiting interaction can be subtracted without changing the whole picture.[22] As a result we have an on-site repulsion of about 5.5 eV, which falls steeply to zero. The extended Hubbard picture has been justified by this reasoning, at least for long polyenes.[19]

In graphite less is known, and the situation is not so clear. In the coronene molecule (which can be considered as a fragment of the graphite layer) the renormalized on-site repulsion is about 8 eV and the limiting value is about 2 eV.[29] Using these data we get the following estimates: $\gamma_0 = 6$ eV, $\gamma_1 = 2.5$ eV. Together with above value of β this corresponds to $U_0 = 2.5$, $U_1 = 1$, which falls into the CDW area on the phase diagram Figure 3.

Relation between Ground State and STM Image of Graphite

In the previous section we obtained a description of the graphite monolayer in different areas of the electronic parameter space. Now let us consider what effect these features of the electronic structure could have on the observed STM image of graphite. According to Tersoff,[10] the observed STM image is the constant conductance surface. The conductance is proportional to $\rho(r, E_F)$, the local density of states (LDOS) of graphite at the Fermi energy:

$$\rho(r, E_F) = \sum_{k,\sigma} [|f_{k\sigma}(r)|^2 \delta(E_F - \epsilon_{k\sigma}^-) + |g_{k\sigma}(r)|^2 \delta(E_F - \epsilon_{k\sigma}^+)] \qquad (17)$$

where $f_{k\sigma}(r)$ and $g_{k\sigma}(r)$ are the occupied and unoccupied orbitals of graphite monolayer, respectively, in the coordinate representation. Since we work in the site representation the coordinate r on the surface can be replaced by an indication of the site (A or B) and of the unit cell number (m, l). The LDOS of graphite is the same for all unit cells (i.e., does not depend on m and l) whereas its dependence on the type of site has the form

$$\sigma(A, E_F) = \sum_{k,\sigma} [|x_{k\sigma}|^2 \delta(E_F - \epsilon_{k\sigma}^-) + |y_{k\sigma}|^2 \delta(E_F - \epsilon_{k\sigma}^+)]$$

$$\sigma(B, E_F) = \sum_{k,\sigma} [|y_{k\sigma}|^2 \delta(E_F - \epsilon_{k\sigma}^-) + |x_{k\sigma}|^2 \delta(E_F - \epsilon_{k\sigma}^+)] \qquad (18)$$

For the graphite monolayer the Fermi surface reduces to two points in reciprocal space: $\pm k_F$ where $k_F = (2\pi/3, -2\pi/3)$. For the metallic phase ($\delta = 0$) the Fermi energy and expansion coefficients are

$$E_F = \gamma_0/2 \qquad |x_{k_F\sigma}|^2 = |y_{k_F\sigma}|^2 = \frac{1}{2}$$

and the upper and lower bands ($\epsilon_{k\sigma}^+$ and $\epsilon_{k\sigma}^-$) are degenerate at k_F. So the LDOS at the A and B sites are equal, $\rho(A, E_F) = \rho(B, E_F)$, and the conductance does not depend on whether the tip is positioned above the A or the B site.

The opposite happens in the case of the CDW ground state. Now the upper and lower bands are separated by a gap, $2(6\gamma_1 - \gamma_0)\delta$. The Fermi energy is

$$E_F = \gamma_0/2 - (6\gamma_1 - \gamma_0)\delta$$

and for that reason only the lower band gives a contribution to the LDOS at the Fermi level. The expansion coefficients for the one-electron state at the Fermi level are

$$|x_{k_F\sigma}|^2 = 1 \qquad |y_{k_F\sigma}|^2 = 0$$

so the LDOS at the A and B sites are not equal $\rho(A,E_F) \neq \rho(B,E_F)$. Now the conductance depends on the position of the tip.

The above picture is closely related to that proposed by Tersoff.[10] The difference is in the treatment of the electronic structure of the graphite monolayer. Our procedure allows us to consider different types of ground states and to reveal their consequences for the STM experiments.

In the SDW state of the graphite monolayer, which has the lowest energy in part of the phase diagram, the charge or the total electron density (and the LDOS as defined by eqs 17 and 18) does not depend on site. The spin density, however, depends on it, and spin-up electrons are largely concentrated on the A sites, whereas spin-down electrons are located preferably on the B sites. Thus graphite in its SDW state is an antiferromagnet. Recently it has been shown that the antiferromagnetic spin structure can reveal itself in the observed STM images, if the tip is ferromagnetic.[30,31] The theory gives the tunneling current between the antiferromagnetic surface and ferromagnetic tip in terms of the local magnetizations of the surface and of the tip.[31] The total tunneling current between the antiferromagnetic surface and the ferromagnetic tip has two contributions:

$$I(r) = I_0 + I_s(r)$$

The first contribution I_0 is half of the sum of the tunneling currents of spin-up and spin-down electrons. It does not depend on the tip position r. The second contribution, $I_s(r)$, describing the spin-dependent part of the tunneling current, is proportional to the product of the local magnetizations of the tip and the surface, $I_s(r) \propto m_t m_s(r)$.

In the SDW state the local magnetization of the graphite monolayer does not depend on the unit cell number. However, it depends on the site within a unit cell, since electrons with opposite spins occupy predominantly different site orbitals. In our notation $m(A) = \delta$, $m(B) = -\delta$, and the spin-dependent part of the tunneling current thus differs for the tip positioned above A and B sites.

So it is possible, at least in principle, to observe not only the charge structure of the graphite surface but its magnetic (spin) structure (if any exists), as well. Unfortunately the experimental work cited[15] does not report what particular tip was used in the studies of a graphite monolayer adsorbed on Pt(111). Nevertheless, careful analysis of the theory[31] reveals that genuine ferromagnetism of the tip is not required to fix the magnetic structure of the surface. What is really required is magnetic polarization of the tip (m_t), which may be of arbitrary origin. For example, if in the one-orbital model of the tip developed by Tersoff and Hamann[32,33] one replaces the single s-orbital used to describe the tip by a pair of corresponding spin-orbitals and takes into account interaction with magnetically polarized electrons by ascribing different energies to the spin-up and spin-down orbitals, the tunneling current is then made up of two unequal terms, corresponding to the tunneling of spin-up and spin-down electrons. If spin-up and spin-down electrons are concentrated on different sites of a lattice (as happens in the case of the SDW graphite layer) the total tunneling current will depend on the position of the tip above the surface, as predicted for the ferromagnetic tip. This may happen even if the material of the tip is not a bulk ferromagnet.

It is usually believed that the STM tip is a single atom or maybe a cluster of a few atoms.[34] At any rate the environment of the atoms in the tip differs dramatically from that in the bulk. That means that the atoms of the tip are closer to the limit of separate high-spin atoms rather than to that of strongly interacting atoms in a probably low-spin solid.[35-37] This may lead to existence of a local magnetic moment in the apical atom of the tip, which in its turn gives rise to an energy difference between the spin-up and spin-down s-orbitals of the tip which are responsible for tunneling.

To summarize the above considerations, we may say that low-symmetry states of both types (SDW and CDW) may be responsible for the observed STM images of the surface of bulk graphite and of the graphite monolayer as well. It seems to us more likely that we observe the CDW state of graphite. However, the possibility of an SDW state cannot be ruled out, since the apical atom of the tip may have a magnetic moment even if the material of the tip is not magnetic.

The results of this paper allow us to look at the STM images of graphite intercalation compounds (GICs)[38,39] from a new perspective. These experiments were designed in order to prove that the observed STM images of neat highly oriented pyrolytic graphite (HOPG) arise from differences in electron density on the A and B sites, which in their turn are driven by the structural differences of these sites in HOPG. Since in the GICs the structural difference between A and B sites in graphite monolayers disappears, the predicted[13,14] STM images of GICs were not supposed to show the normally seen period of 2.46 Å, corresponding to observation of only three atoms of the six (see above). The outcome of the experiments,[38,39] however, was disappointing. The STM images of stage-1 GIC KC$_8$ still bear features with a period of 2.46 Å, as in the STM images of HOPG and the graphite monolayer on Pt(111). This residual structural pattern exists in addition to the main structure with a period of 4.9 Å (which matches the K–K separation in the KC$_8$ GIC), though the structural asymmetry between the A and B sites of graphite layers is removed in GICs.

If we accept that the only effect of intercalation on the graphite monolayer is transfer of electrons from potassium (or other alkaline-metal atoms) to the π-bands of the latter, we can describe the electronic structure of the negatively charged monolayer with use of the same self-consistency equations eqs 9, 10, and 14. Additional electrons change the integration limits in eqs 9 and 14, but the structure of the self-consistency equations does not change. One can still find ground states of both CDW and SDW types for the band filling characteristic of the GICs, as well as for the neat graphite monolayer. The LDOSs on A and B sites in the CDW state are also different in the charged monolayer. These differences are driven not by structural reasons, which are clearly absent in the case of GICs, but by the electronic structure of the graphite monolayer itself. This is not to say that we have provided a complete interpretation of the STM images of GICs, which are quite complex.

It should be noted that the original reasoning due to Tersoff seems to be unable to cover the case of GICs. After the electrons are dumped from the alkaline-metal atoms into the graphite monolayer the latter is no longer a gapless semiconductor. For that reason qualitative considerations based on particular features of the Fermi surface do not apply any more, whereas the solutions of the self-consistency equations (eqs 7 and 9) with proper integration limits) describe the electronic structure of the GICs and can give a ground state of the unsymmetric (SDW or CDW) type.

References and Notes

(1) Sugihara, K.; Spain, I. L.; Goldberg, H. *Graphite Fibers and Filaments*; Springer Series in Materials Science; Springer-Verlag: Berlin, 1988; Vol. 5.

(2) Brandt, N. B.; Chudinov, S. M.; Ponomarev, Ya. G. Semimetals, Graphite and its Compounds. *Modern Problems in Condensed Matter Sciences;* North-Holland: Amsterdam, 1988; Vol. 20.1.

(3) Davis, S. M.; Somorjai, G. A. In *The Chemical Physics of Solid Surfaces and Heterogeneous Catalysis;* King, D. A., Woodruff, D. P., Eds.; Elsevier: Amsterdam, 1983; Vol. 4.

(4) Horsley, J. A. In *Chemistry and Physics of Solid Surfaces;* Vanselow, R., Howe, R., Eds.; Springer: Berlin, 1990; Vol. 8.

(5) Binnig, G.; Fuchs, H.; Gerber, Ch.; Rohrer, H.; Stoll, E.; Tosatti, E. *Europhys. Lett.* **1986,** *1,* 31.

(6) Park, S.-I.; Quate, C. F. *Appl. Phys. Lett.* **1986,** *48,* 112.

(7) Soler, A. M.; Baro, N.; Garcia, J. M.; Rohrer, H. *Phys. Rev. Lett.* **1986,** *57,* 444.

(8) Hansma, P. K. *Bull. Am. Phys. Soc.* **1985,** *30,* 251. Kuwabara, M.; Clarke, D. R.; Smith, D. A. *Appl. Phys. Lett.* **1990,** *56,* 2396.

(9) Sugawara, Y.; Ishizaka, T.; Morita, S. *Jpn. J. Appl. Phys.* **1990,** *29,* 1539.

(10) Tersoff, J. *Phys. Rev. Lett.* **1986,** *57,* 440.

(11) Slonczewski, J. C.; Weiss, P. R. *Phys. Rev.* **1958,** *109,* 272.

(12) McClure, J. W. *Phys. Rev.* **1957,** *108,* 612.

(13) Tomanek, D.; Louie, S. G. *Phys. Rev. B* **1988,** *37,* 8327.

(14) Tomanek, D.; Louie, S. G.; Mamin, H. J.; Abraham, D. W. Thomson, R. E.; Clarke, J. *Phys. Rev. B* **1987,** *35,* 7790.

(15) Land, T. A.; Michely, T.; Behm, R. J.; Hemminger, J. C.; Comsa, G. *Surf. Sci.* **1992,** *264,* 261.

(16) Ashcroft, N. W.; Mermin, N. D. *Solid State Physics;* W. B. Saunders Co.: Philadelphia, 1976.

(17) Hoffmann, R. *Solids and Surfaces: A Chemist's View of Bonding in Extended Structures;* VCH: New York, 1988.

(18) Misurkin, I. A.; Ovchinnikov, A. A. *Teor. Eksp. Khim.* **1968,** *4,* 3 (in Russian); *Theor. Exp. Chem.* **1968,** *4,* 3 (in English).

(19) Hayashi, H.; Nasu, K. *Phys. Rev. B* **1985,** *32,* 5295. Belinskii, A. E.; Tchougreeff, A. L.; Misurkin, I. A. *Teor. Eksp. Khim.* **1989,** *25,* 513 (in

Russian); *Theor. Exp. Chem.* **1989,** *25,* 475 (in English). Tchougreeff, A. L.; Misurkin, I. A. *Zh. Strukt. Khim.* **1989,** *30,* No 3, 24 (in Russian); *J. Struct. Chem.* **1989,** *30,* 377 (in English).

(20) Hückel, E. *Z. Phys.* **1931,** *70,* 204; *Ibid.* **1931,** *72,* 301; *Ibid.* **1932,** *76,* 628.

(21) Dewar, M. J. S. *The PMO Theory of Organic Chemistry;* Plenum: New York, 1975.

(22) Misurkin, I. A.; Ovchinnikov, A. A. *Usp. Khim.* **1977,** *46,* 1835 (in Russian); *Russ. Chem. Rev.* **1977,** *46,* 967 (in English).

(23) Solyom, J. *Adv. Phys.* **1979,** *28,* 201.

(24) Misurkin, I. A.; Ovchinnikov, A. A. *Teor. Eksp. Khim.* **1976,** *12,* 291 (in Russian); *Theor. Exp. Chem.* **1976,** *12,* 225 (in English).

(25) Peacock, T. E. *Electronic Properties of Aromatic and Heterocyclic Molecules;* AP: London, 1965.

(26) Coulson, C. A.; Taylor, R. *Proc. Phys. Soc.* **1952,** *A65,* 815.

(27) Weiss, C.; Kobayashi, H.; Gouterman, M. *J. Mol. Spectrosc.* **1965,** *16,* 415.

(28) Schug, J.; Reid, R. D.; Lilly, A. C.; Dwyer, R. W. *Chem. Phys. Lett.* **1986,** *128,* 5.

(29) Gutfreund, H.; Little, W. A. *Phys. Rev.* **1969,** *183,* 68.

(30) Wiesendanger, R.; Guntherodt, H. J.; Guntherodt, G.; Gambino, R. J.; Rut, R. *Phys. Rev. Lett.* **1990,** *65,* 247.

(31) Molotkov, S. N. *Surf. Sci.* **1992,** *261,* 7.

(32) Tersoff, J.; Hamann, D. R. *Phys. Rev. Lett.* **1983,** *50,* 1998.

(33) Tersoff, J.; Hamann, D. R. *Phys. Rev. B* **1985,** *31,* 805.

(34) Tsukada, M.; Kobayashi, K.; Isshuki, N.; Kageshima, H. *Surf. Sci. Rep.* **1991,** *13,* 265.

(35) Himpsel, F. J. *J. Magn. Magn. Mater.* **1991,** *102,* 261.

(36) Fu, C. L.; Freeman, A. J.; Oguchi, T. *Phys. Rev. Lett.* **1985,** *54,* 2700.

(37) Richter, R.; Gay, J. G.; Smith, J. R. *Phys. Rev. Lett.* **1985,** *54,* 2704.

(38) Kelty, S. P.; Leiber, C. M. *J. Phys. Chem.* **1989,** *93,* 5983.

(39) Kelty, S. P.; Lieber, C. M. *Phys. Rev. B* **1989,** *40,* 5856.

Photoinduced Changes in the Se–Ag–I System

M. Mitkova,* T. Petkova, P. Markovski, and V. Mateev

Central Laboratory of Optical Storage and Processing of Information, Bulgarian Academy of Sciences, Sofia 1113, P.O. Box 95, Bulgaria (Received: May 12, 1992; In Final Form: July 14, 1992)

Photoinduced changes in thin films from the Se–Ag–I system are investigated firstly, employing various methods—holography, microscopy, electron microscopy, X-ray analysis, and Auger electron spectroscopy. The influence of the composition on the photoinduced changes, as well as the possibility of inducing considerable photoanisotropy, is demonstrated. The mechanism of the processes is discussed on the basis of the experimental data, the phenomena being related to Weigert effect in silver halide systems, photocrystallization, and orientation of defects in chalcogenide systems.

Introduction

The amorphous semiconductors are a very attractive material because of their great potential applicability.[1] The photoinduced changes, especially typical of chalcogenide glassy materials, allow reversible[2] and irreversible[3] optical recording in them. Alongside with the photoinduced changes of the absorption coefficient and the refractive index, photoinduced anisotropy is also observed.[4] Optical recording in these materials does not need subsequent processing. Besides, they possess good chemical resistance in aggressive ambients and high transmittance in the near-IR region. In recent years the researchers' interest has been drawn to the synthesis and investigations of a new chalcogenide–halide family of materials for fiber optics.[5]

The investigations on chalcogenide–halide glasses of the Se–Ag–I system[6] give grounds to expect that they are suitable for holographic recording combining the good transmittance in the IR region of the halide materials with the photosensitivity of the chalcogenides.

The objective of the present work is to investigate the photoinduced changes in this system and the possibilities for applying them as an optical recording medium, using various investigation methods—holography, microscopy, electron microscopy, X-ray analysis, and Auger electron spectroscopy.

Experimental Section

The investigated films with a thickness of 500–1000 nm were prepared by vacuum thermal evaporation.[7] The specimens were left in darkness for 24 h in order to eliminate the possible influence of their thermal history.

The chemical composition of the thin films was investigated by Auger electron spectroscopy. The transmission spectra of Ar^+ laser irradiated and nonirradiated samples were studied in the spectral range 400–2500 nm.

The experimental setup for holographic recording is shown in Figure 1. A continuous Ar^+ laser with a wavelength $\lambda = 488$ nm in a standard interferometric configuration produces fringes with a spatial frequency 200 mm^{-1}. The intensity of the interfering beams is controlled with a gradual attenuator. The substrate holder temperature is maintained constant by a thermostat at 20 $\pm$ 1 °C. During recording the diffraction efficiency is measured with a linearly polarized He–Ne laser beam with a wavelength $\lambda = 632.8$ nm. The local heating at the area of recording is measured with a copper–constantan thermocouple.

The holographic scalar recording is carried out with two equal circular (left-hand or right-hand rotating) polarizations. The recording beam's intensity is 2.5 W/cm^2. The resulting interference pattern has a circular polarization and intensity, varying by a sinusoidal law.

The polarization holographic recording permits the reconstruction of both the intensity distribution of the wavefront and the recording wave polarization.[8] The polarization recording with two orthogonal circularly (left-hand and right-hand rotating) polarized Ar^+ laser beams is accomplished by the arrangement in Figure 1, removing the $\lambda/2$ phase plate. In this case the